GEOLOGICAL JOURNAL
Geol. J. **49**: 635–648 (2014)
Published online 23 May 2014 in Wiley Online Library
(wileyonlinelibrary.com). DOI: 10.1002/gj.2573

Geology, fluid inclusion and age constraints on the genesis of the Sarekuobu gold deposit in Altay, NW China

LI ZHANG[1], HUA-YONG CHEN[1]*, YI ZHENG[2], YA-JING QIN[1] and DENG-FENG LI[1]

[1] *Key Laboratory of Mineralogy and Metallogeny, Guangzhou Institute of Geochemistry, Chinese Academy of Sciences, Guangzhou, China*
[2] *Department of Earth Sciences, Sun Yat-sen University, Guangzhou, China*

The Sarekuobu gold deposit was discovered in the 1990s and is located in the Kelan Basin on the southern margin of the Chinese Altay Orogen. Orebodies are hosted in the Early Devonian metamorphosed volcanic-sedimentary sequence and controlled by the NW-trending Abagong Fault. Mineralization can be divided into early, middle and late stages, characterized by quartz–pyrite, polymetallic quartz–sulphides and carbonate–quartz, respectively. Four types of fluid inclusions were identified in quartz veins, i.e. pure CO_2 (PC-type), CO_2–H_2O (C-type), aqueous (W-type) and daughter mineral-bearing inclusions (S-type). Hydrothermal fluids related to the mineralization are composed of CO_2–H_2O–NaCl ± CH_4 ± N_2 fluids with T_h values of 236–374 °C and salinities of 4.8–15.0 wt.% NaCl eqv. (in general 8.0–15.0 wt.% NaCl eqv.), combined with trapping pressures of 90–330 MPa, suggesting that the mineralization resulted from a metamorphic fluid system. One biotite sample from the polymetallic quartz lodes yields a $^{40}Ar/^{39}Ar$ isotopic plateau age of 213.5 ± 2.3 Ma, marking the time of mineralization as Triassic. This mineralization age is broadly comparable with the mineralization age reported from the Tiemurt Pb–Zn deposit and Wulasigou Cu deposit located near the Sarekuobu gold deposit, indicating that the deposit was possibly related to the Permian–Triassic continental collision at the southern margin of the Altay Orogen. Our results show that the Sarekuobu gold deposit is not syngenetic, but an epigenetic orogenic gold deposit.

Received 18 November 2013; accepted 28 April 2014

KEY WORDS Sarekuobu gold deposit; fluid inclusion; biotite Ar–Ar geochronology; Altay Orogen; NW China

1. INTRODUCTION

The Sarekuobu gold deposit contains estimated reserves of 8 t gold at an average grade of 3.86 g/t and is distributed in the Abagong polymetallogenic belt in the south of the Altay Orogen, in which the major ore deposits, including the Tiemurt Pb–Zn deposit, Wulasigou and Qiaxia Cu deposits and Sarekuobu Au deposit, are hosted by Devonian metamorphosed volcano-sedimentary rocks of the Kangbutiebao Formation.

The origins of these deposits and the mechanism for such giant accumulations of Pb, Zn, Cu and Au have long been controversial. The CO_2-rich, low-salinity fluids combining with other ore geological characteristics (e.g. the orebodies controlled by faults or shear zones) have led some researchers (Xu *et al*., 2008; Qin *et al*., 2012; Zheng *et al*., 2012; Zhang *et al*., 2012b; Zheng *et al*., 2013, 2014) to include these deposits in an orogenic class, as defined by Groves *et al*. (1998) and to conclude that these deposits are epigenetic which are related to the Permian–Triassic continental collision. Ar–Ar ages of 240–219 Ma obtained by Zheng *et al*. (2012, 2013) on ore-related mica from the Tiemurt Pb–Zn and Wulasigou Cu deposits appear to support the epigenetic origin of mineralization, as well as a link with metamorphism that occurred in the Abagong region during this period. However, some authors (e.g. Wang *et al*., 1998; Ding *et al*., 2001; Tong, 2007; Wang *et al*., 2007) have classified the Sarekuobu gold deposit as syngenetic volcano-sedimentary type (i.e. VMS type) based on its stratabound character and the Rb–Sr isochron age of 395 ± 39 Ma from hydrothermal quartz (Li *et al*., 2004), which is similar to the Kangbutiebao Formation host volcanic rocks that yield SHRIMP U–Pb ages ranging from 421 to 396 Ma (Chai *et al*., 2009; Shan *et al*., 2012; Zheng *et al*., 2013). Nonetheless, this Rb–Sr age is considered, in general, as non-robust dating, so that the relationship between mineralization and host rocks remains undemonstrated.

*Correspondence to: H.-Y. Chen, Guangzhou Institute of Geochemistry, Chinese Academy of Sciences, 511 Kehua Street, Tianhe District, Guangzhou 510640, Guangdong, China. E-mail: huayongchen@gig.ac.cn

Recent geologic, fluid inclusion and Ar–Ar dating data on the Tiemurt Pb–Zn and Wulasigou Cu deposits in the Abagong belt raise interesting aspects, such as that the ages of the main mineralization event are much younger than that of the host rocks and that ore-forming fluids may not have a significant link to seawater but instead to metamorphic or deep-sourced fluids (Xu *et al*., 2008, 2011; Wang *et al*., 2012; Zheng *et al*., 2012; Zhang *et al*., 2012b).

In this paper, we describe in detail the regional and local geology of the Sarekuobu gold deposit, followed by fluid inclusion and Ar–Ar dating data. A discussion on the genesis of this deposit is then presented to approach an ore-forming model for the metallogenesis of the Abagong polymetallic belt.

2. REGIONAL GEOLOGY

The Central Asian Orogenic Belt (CAOB) is an orogenic collage comprising ophiolite suites, magmatic arcs, Precambrian microcontinental massifs and several accretionary terranes, which resulted from the collision between the Siberia and Tarim-SinoKorean plates along the Solonker Suture that progressively closed eastward from the end of the Early Carboniferous to the Early Triassic (Sengor and Natal'in, 1996; Chen *et al*., 2007a, 2009; Xiao *et al*., 2009; Chen *et al*., 2012). In spite of this diachronous oceanic closure, the CAOB is generally accepted as a Late Palaeozoic (320–256 Ma) or Hercynian (Variscan) collisional orogenic belt (Y.J. Chen *et al*., 2012).

The Altay Orogen extends for more than 2500 km from Kazakhstan, parts of Russia, across northwest China (Xinjiang) to western Mongolia, and was formed through a complex series of events that include accretion, subduction and opening and closing of small basins (Chen, 2000; Goldfarb *et al*., 2003; Xiao *et al*., 2009). As the northernmost part of Xinjiang, the Chinese Altay is an accretionary complex onto the southern margin of the Siberia continental plate, with the Ertix (also spelled as Irtysh, Erqis or Yrtys) tectonic suture as its southern boundary (Fig. 1) which hosts an orogenic-type gold belt (Chen *et al*., 2001).

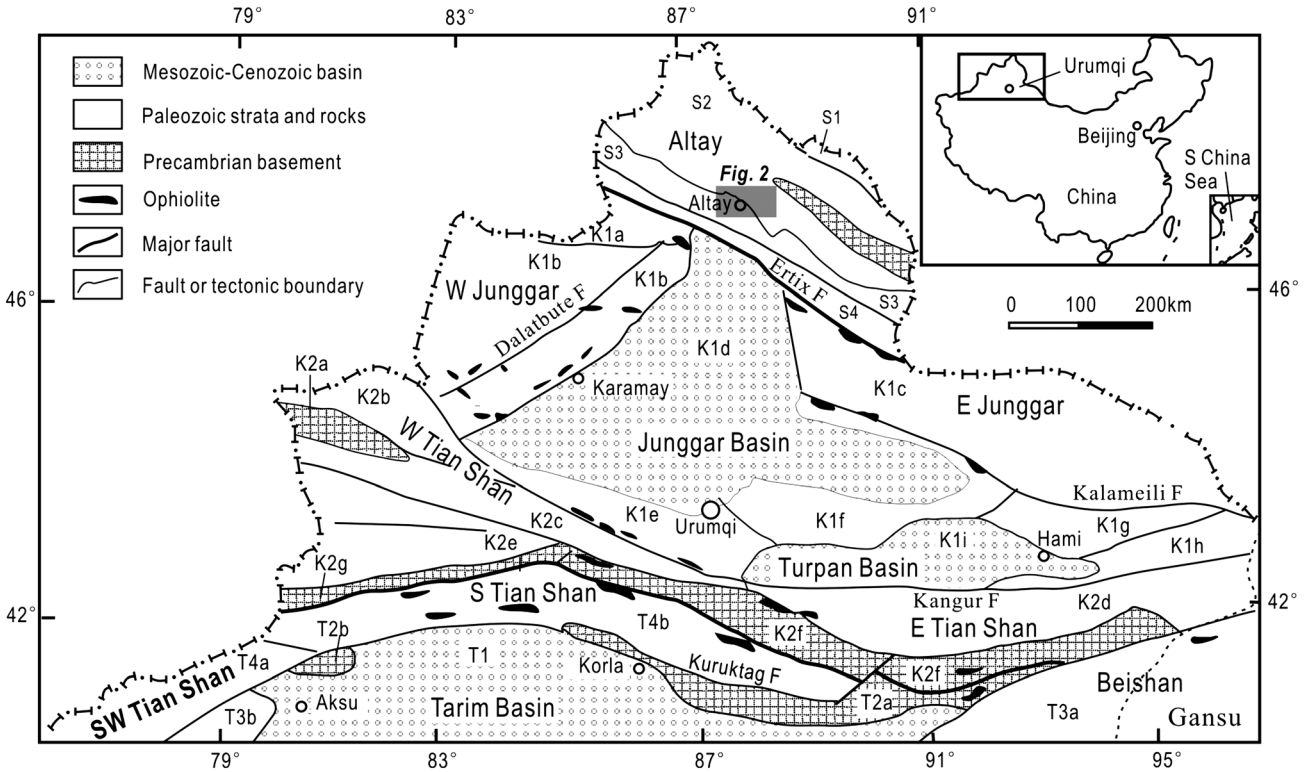

Figure 1. Sketch map showing tectonic framework of North Xinjiang (Y.J. Chen *et al*., 2012) Siberia Plate: S1, Nurt Late Devonian–Early Carboniferous volcanic basin; S2, Keketuohai Palaeozoic magmatic arc; S3, Kelan Devonian–Carboniferous fore-arc basin; S4, Armantay-Irtysh accretionary wedge. Kazakhstan Plate: K1a, Zharma-Sawur island arc; K1b, Western Junggar accretionary complex; K1c, Eastern Junggar accretionary complex; K1d, Junggar Mesozoic–Cenozoic basin; K1e, Yelianhabirga Late Palaeozoic back-arc basin; K1f, Bogada Late Palaeozoic aulacogen; K1g, Harlike Palaeozoic island arc; K1h, Dananhu island arc; K1i, Turpan Mesozoic–Cenozoic basin; K2a, Sailimu massif; K2b, Wenquan terrane; K2c, Boloholo Palaeozoic arc-basin system; K2d, Yamansu-Jueluotag Palaeozoic arc-basin system; K2e, Ili Carboniferous–Permian rift; K2f, central Tianshan Early Palaeozoic island arc with Precambrian fragments; K2g, Nalati massif. Tarim Plate: T1, Tarim Mesozoic–Cenozoic basin; T2a, Kuruktag Precambrian massif; T2b, Muzart massif; T3a, Beishan Carboniferous–Permian aulacogen; T3b, Kalatierek Late Palaeozoic passive marginal sediments; T4a, Southwest Tianshan Late Palaeozoic fold-and-thrust belt; T4b, Southern Tianshan (or Kumishi) Palaeozoic accretionary complex.

The Sarekuobu gold deposit is hosted in the Devonian Kelan volcano-sedimentary basin. The basement of the Kelan Basin consists of the Mesoproterozoic Kemuqi and Neoproterozoic Fuyun groups, which are composed variably of gneisses, migmatites and marbles. In the studied area, the Kelan Basin is composed of a series of multiple overturned synclines that strike for 50 km with axial planes dipping northwest. The sedimentary strata exposed in the studied area consist of the Middle to Upper Silurian Kulumuti Group, the Lower Devonian Kangbutiebao Formation and the Middle Devonian Altay Formation. The Kulumuti Group comprises biotite gneiss, migmatites and quartz–biotite schist, which is unconformably overlain by the Lower Devonian Kangbutiebao Formation and Middle Devonian Altay Formation in ascending sequence. The Kangbutiebao Formation consists of meta-rhyolite, meta-andesite, quartz schist, meta-arenite, pyroxenite and marble. SHRIMP U–Pb ages on zircons from meta-rhyolite range from 421 to 396 Ma (Chai *et al.*, 2009; Shan *et al.*, 2012; Zheng *et al.*, 2013). Most researchers believe the Kangbutiebao Formation was erupted and deposited in a volcanic arc system (Goldfarb *et al.*, 2003) or rifting environment (Chai *et al.*, 2009). The Altay Formation is dominated by meta-arenite and greywacke with volcanic arenite intercalations. The Devonian volcanic and sedimentary rocks underwent metamorphism from middle greenschist to lower amphibolite facies, and metamorphic mineral assemblages are composed of quartz + biotite + chlorite + epidote + actinolite. The Kangbutiebao Formation hosts, besides Sarekuobu, other important mineral deposits of the Abagong polymetallic belt, such as the Pb–Zn deposits of Tiemurt, Talate and Dadonggou and the Cu deposits of Wulasigou and Qiaxia (Fig. 2).

The intermediate to felsic intrusions are widespread in the Altay Orogen, ranging from the Ordovician, through the Permian, to the Triassic and even to the Early Jurassic in age.

Faults in the Kelan Basin run roughly NW–SE and mark the boundaries of different stratigraphic units. The Keyingong and Hongdun faults separate the Silurian and Devonian strata, whilst the Abagong and Altay faults separate the Kangbutiebao and Altay formations. The Abagong Fault also controls the location of all the polymetallic deposits, e.g. the Dadonggou, Tiemurt, Abagong Pb–Zn deposits, the Wulasigou, Qiaxia Cu deposits and the Sarekuobu Au deposit.

3. ORE GEOLOGY

The Sarekuobu gold deposit lies 10 km northwest of the town of Altay and was discovered in the middle 1990s. The geographical coordinates of the Sarekuobu gold deposit is 88°12′43″E–88°14′17″E longitude and 47°52′04″N–47°

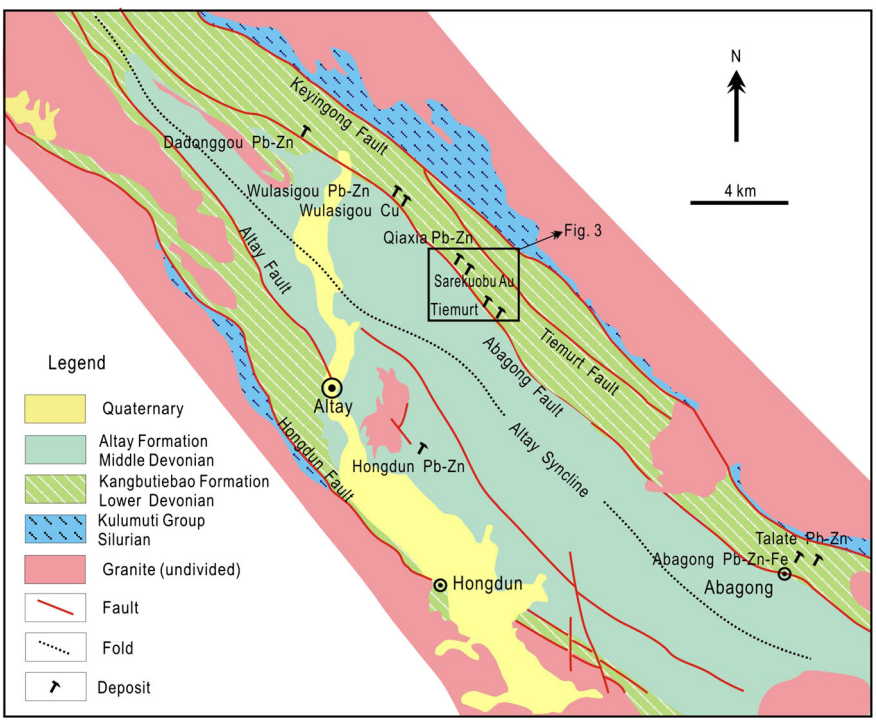

Figure 2. Geological map of the Abagong ore belt (modified after Geological Team 706 of the Xinjiang Bureau of Nonferrous Metals, 2000). This figure is available in colour online at wileyonlinelibrary.com/journal/gj

53′12″N latitude, with a total mine area of about 3 km^2. The orebodies are hosted in the greenschist–amphibolite facies Upper Kangbutiebao Formation, which includes meta-rhyolitic tuff, chlorite–quartz schist and marble. No intrusive rocks have been observed within or adjacent to the deposit (Figs. 3 and 4). The Abagong Fault controlled the Au mineralization in the mining area and the associated shear zone striking 71–80° and dipping northeast at 45–55°.

The Sarekuobu gold deposit consists of four main orebodies (No. 1-1, No. 1-2, No. 2 and No. 3) (Figs. 3 and 4), among which, lode No. 1-1 is the largest and most representative. The gold vein of No. 1-1 occurs in the southern wing of the northeast-verging Sarekuobu overturned anticline. It is 462 m in length and 1.85–3.32 m in thickness, with a gold grade of 1.20–16.57 g/t (mean = 3.68 g/t). Lode No. 1-2, the second largest gold vein, is situated in the southeast of the lode No. 1-1. The lode No. 1-2 is 120 m long and 1.51–3.01 m thick, with a grade of 2.91–11.26 g/t (mean = 4.28 g/t), dipping to 40–50° with angle of 76–79° (Fig. 4). Most orebodies are lenticular or vein type. They are generally NW-trending and parallel to each other, controlled by a shear zone (Fig. 5A) and locally showing an *en echelon* appearance (Fig. 5B).

Two styles of gold mineralization are distinguished at the Sarekuobu deposit: the most common are gold-bearing quartz vein/veinlet stockworks (Fig. 5C, D) and a small portion of disseminated gold in the altered host rocks. The ore minerals are mainly chalcopyrite, pyrite, pyrrhotite, sphalerite, galena and some native gold, and the gangue minerals are quartz, biotite, chlorite, epidote, fluorite and calcite. Besides vein textures, some ores with laminated, massive and disseminated textures have also been recognized.

Within the ore zones, the hydrothermal alteration is characterized by silicification, biotitization, chloritization, epidotization, carbonation, fluoritization and intensive sulphidization. The contact between auriferous quartz veins and the wall rocks is sharp, although alteration zones with pyrite–quartz veinlets and disseminated sulphides may develop outside of the main veins.

At least three stages of quartz veins are recognized. The first stage consists of sigmoidal vein arrays, which were structurally deformed, brecciated, mylonitized and recrystallized in ductile to ductile-brittle shear zones. Quartz in this stage is characterized by undulose extinction and pronounced subgrain formation which indicate intracrystalline deformation (Fig. 5E). Sulphides in this stage, dominated by pyrite, are not economically important. The second-stage veins infilled fractures in the early-stage veins

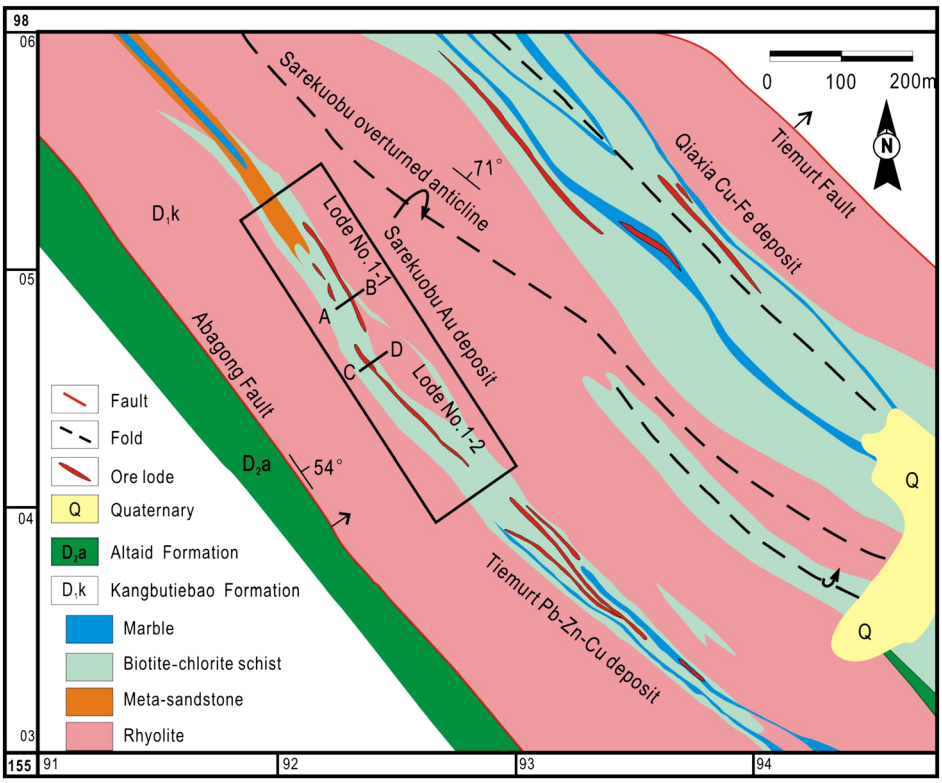

Figure 3. Geological map of the Sarekuobu gold deposit (modified after Geological Team 706 of the Xinjiang Bureau of Nonferrous Metals, 2000). This figure is available in colour online at wileyonlinelibrary.com/journal/gj

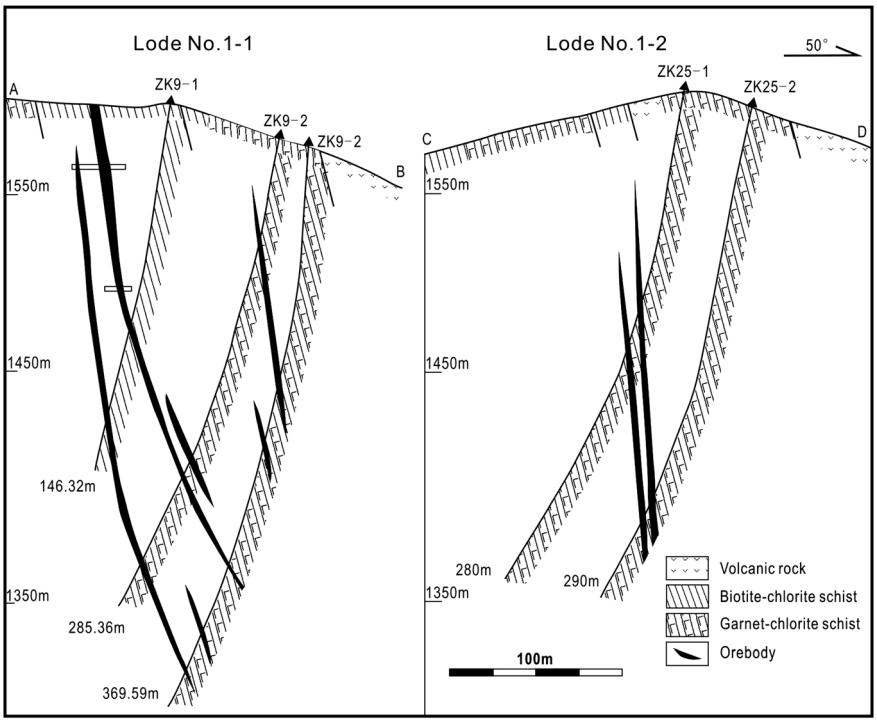

Figure 4. Geological profiles of Nos. 1-1 and 1-2 prospecting lines in the Sarekuobu gold deposit (modified after Geological Team 706 of the Xinjiang Bureau of Nonferrous Metals, 2000).

and alteration assemblages and are usually undeformed, suggesting a dilational shear setting. Representative minerals in the second stage include pyrite, chalcopyrite, pyrrhotite, quartz, sericite, epidote, chlorite and fluorite (Fig. 5C, D, F, G). Some of these veins show a laminated texture, locally containing wall-rock breccias, probably indicating a fault-valve behaviour under brittle-ductile conditions, facilitated by episodic hydraulic fracturing in the fluid conduit. The veins in this stage are of great importance because native gold and electrum were observed under reflected-light microscopy. The third stage is characterized by quartz and carbonate veins or veinlets (Fig. 5H), which cross-cut the earlier formed veins, stockworks and altered rocks.

4. FLUID INCLUSIONS

4.1. Samples and analytical methods

A total of 14 samples of quartz vein-type ores were collected from No. 1-1 orebody; 20 double-polished thin sections (about 0.20 mm thick) were made and selected for microthermometric and Raman microprobe analyses.

Microthermometric measurement was performed using a Linkam TH600 heating–freezing stage attached to a Leitz Ortholux transmitted light microscope connected with a television camera and screen at the Guangzhou Institute of Geochemistry, Chinese Academy of Sciences. The heating rate was maintained from 0.2 to 5 °C/min but reduced to less than 0.2 °C when close to phase change conditions. The stage was calibrated using the standard of synthetic fluid inclusions. Estimated accuracy was ±0.1 °C at temperature below 30 °C and ±1 °C at temperature above 30 °C. Salinities were calculated using the equations of Bodnar (1993) for H_2O–NaCl inclusions and Collins (1979) for CO_2–H_2O inclusions, respectively, which were expressed as weight per cent NaCl equivalents. Salinities of daughter mineral-bearing inclusions were calculated using the dissolution temperatures of daughter minerals (Hall *et al*., 1988).

4.2. Fluid inclusion types and characteristics

Four types of fluid inclusions were recognized in quartz on the basis of phases present at room temperature and phase changes during heating and cooling (Fig. 6).

(1) CO_2–H_2O fluid inclusions (C-type). C-type inclusions consist of either two phases (liquid H_2O + liquid CO_2) or in some cases three phases (liquid H_2O + liquid CO_2 + vapour CO_2) at room temperature. C-type fluid inclusions appear ellipsoidal or irregular in shape, with

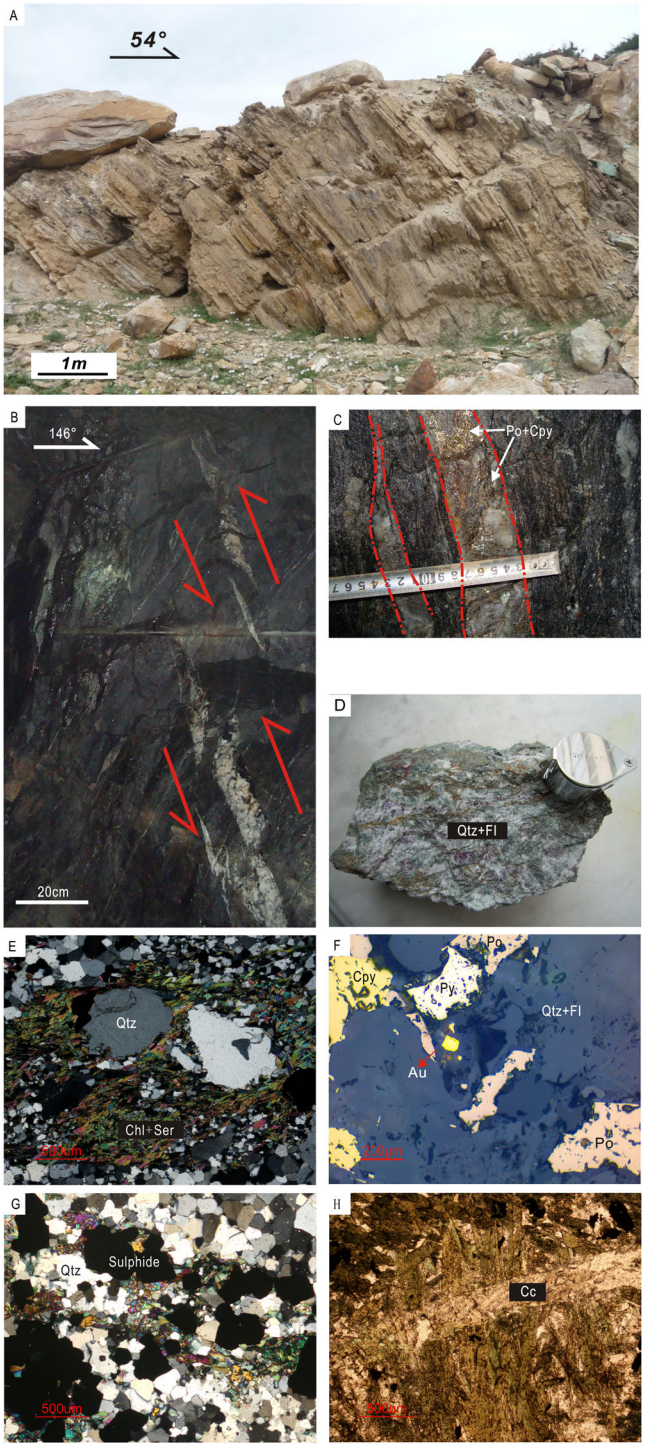

Figure 5. Photos showing the ore geology of the Sarekuobu gold deposit: (**A**) shear zone in the Sarekuobu gold deposit; (**B**) veins controlled by *en echelon* cutting across the banded quartz veins in the footwall; (**C**) middle-stage quartz veins containing sulphides; (**D**) quartz and fluorite vein in the middle stage; (**E**) early-stage quartz with undulose extinction and subgrain formation; (**F**) middle-stage sulphides associated with native gold; (**G**) middle-stage fine-grained quartz associated with sulphides (**H**) late-stage calcite veinlet cutting chlorite-altered wall rocks. Abbreviations: Po—pyrrhotite; Cpy—chalcopyrite; Py—pyrite; Au—native gold; Qtz—quartz; Fl—fluorite; Chl—chlorite; Ser—sericite; Cc—calcite. This figure is available in colour online at wileyonlinelibrary.com/journal/gj

sizes ranging from 4 to 20 μm. The carbonic phase (V_{CO2} or $V_{CO2}+L_{CO2}$) occupies 15–80 vol.% of the inclusions at room temperature. C-type fluid inclusions occur as isolated individual inclusions, locally in clusters (Fig. 6A, B), and they are most abundant in the four types, making up more than 40% of all primary inclusions.

(2) Pure carbonic fluid inclusions (PC-type). PC-type inclusions range in size from 7 to 15 μm and consist of a single phase (liquid CO_2 or vapour CO_2) or two phases (liquid CO_2 + vapour CO_2) at room temperature. No visible liquid water was found in these inclusions. They commonly have sub-rounded or irregular shapes and are distributed in clusters with C-, W- and S-type inclusions (Fig. 6C).

(3) Aqueous fluid inclusions (W-type). W-type inclusions consist of two-phase aqueous inclusions, consisting of vapour and liquid water at room temperature. They occur mostly in clusters, in intergranular trails and locally as isolated individual inclusions. W-type inclusions are negative crystals or sub-rounded in shape and 4–10 μm in size, with $V_{H2O}/(L_{H2O}+V_{H2O})$ ranging between 5–25 vol.% (Fig. 6C). Some inclusions occur along healed fractures that cut across different quartz grains and have highly irregular, elongate or tabular shapes and are considered as secondary in origin (Fig. 6D).

(4) Daughter mineral-bearing inclusions (S-type). They are rare and consist of a liquid, a vapour phase and one or two daughter minerals. The daughter minerals are mainly cubic halite (Fig. 6E) and in some cases round sylvite; in addition, some unidentified daughter crystals and an opaque mineral are present in a few inclusions. S-type inclusions are irregular, ellipsoidal and isolated, with size varying between 6 and 10 μm.

In the early-stage samples, the majority of inclusions are C- and PC-type inclusions with fewer W-type fluid inclusions. All four types of fluid inclusions occur in the middle stage, although we noted that the predominant types of inclusions in this stage are C- and PC-types. In late-stage samples, only W-type inclusions were observed.

4.3. *Microthermometry*

The microthermometric data of the fluid inclusions are obtained from the primary fluid inclusions, and they are summarized in Table 1 and plotted in Figure 7.

The C-type fluid inclusions are dominant in the early stage. The melting temperatures of solid CO_2 ($T_{m,CO2}$) of C-type inclusions range from −68.5 to −56.6 °C, with most below the triple-phase point (−56.6 °C) of CO_2, suggesting minor amounts of dissolved components in the carbonic

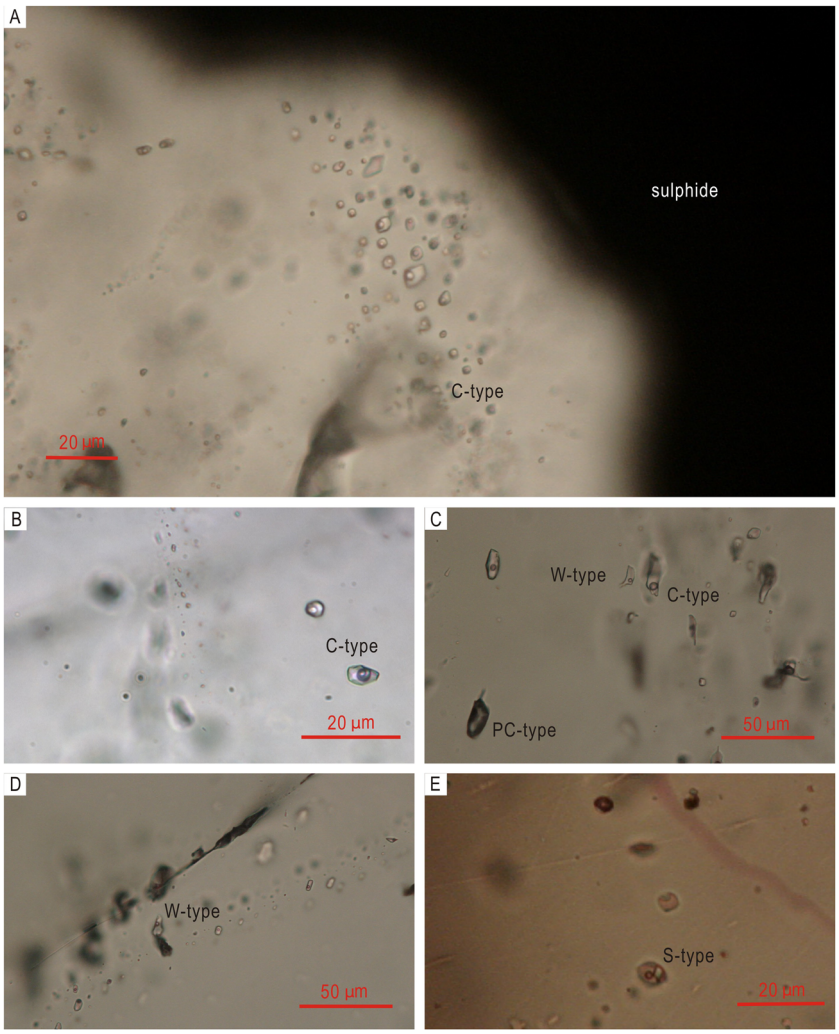

Figure 6. Photomicrographs of fluid inclusions: (**A**) primary inclusions trapped in the middle-stage hydrothermal quartz. Primary inclusions occur as isolated individuals and in clusters. Note that the quartz grains share common grain boundaries with sulphides; (**B**) the C-type fluid inclusion; (**C**) a cluster of PC-, C- and W-type inclusions trapped in the middle-stage quartz; (**D**) W-type fluid inclusions along the healed fracture; (**E**) isolated S-type fluid inclusions. This figure is available in colour online at wileyonlinelibrary.com/journal/gj

phase. The clathrate melting temperatures ($T_{m,cla}$) are between 5.4 and 6.9 °C, corresponding to salinities between 5.9 and 8.4 wt.% NaCl eqv. The C-type fluid inclusions show total homogenization temperatures (T_h) ranging from 271 to 446 °C. The carbonic phase homogenized to vapour at temperatures from 9.4 to 24.7 °C ($T_{h,CO2}$), corresponding to densities from 0.82 to 0.98 g/cm^3. PC-type inclusions contain only liquid CO_2 or liquid CO_2 + vapour CO_2 at room temperature, but a vapour bubble occurred during cooling runs. These inclusions yield melting temperatures for solid CO_2 from −69.1 to −56.6 °C, suggesting a possible presence of small contents of other gases such as CH_4 or N_2, which were detected by Raman spectroscopy analysis (see below). The homogenization temperatures of CO_2 to the liquid phase show a large variation from −20.3 to 20.7 °C, corresponding to densities from 0.76 to 1.03 g/cm^3.

In the middle stage, the C-type fluid inclusions yield solid CO_2-melting temperatures of mainly −62.0 to −57.3 °C, suggesting a small quantity of other gases dissolved in the carbonic phase. Clathrate melting temperatures range from 2.3 to 6.9 °C, corresponding to salinities of 5.9–12.8 wt.% NaCl eqv. The total homogenization temperatures range from 257 to 374 °C. The carbonic phase homogenized to vapour at temperatures from 7.2 to 27.9 °C, corresponding to densities from 0.76 to 1.03 g/cm^3. The W-type inclusions yield ice-melting temperatures ($T_{m,ice}$) from −11.0 to −2.9 °C, with salinities ranging from 4.8 to 15.0 wt.% NaCl eqv. Most of the W-type inclusions are homogenized to liquid or vapour at temperatures of 236–373 °C, with densities of 0.78–0.93 g/cm^3. In the S-type fluid inclusions, vapour bubbles disappear at temperature of 167–243 °C, and halite daughter minerals dissolve at temperatures of 245–314 °C, corresponding to

Table 1. Microthermometry data of fluid inclusions of different mineralization stages

Stage	Type	*n*	$T_{m,CO2}$/°C	$T_{m,cla}$/°C	$T_{h,CO2}$/°C	$T_{m,ice}$/°C	T_h/°C	wt.% NaCl eqv.
Early	PC	42	−69.1 to −56.6		−20.3 to 20.7			
	C	58	−68.5 to −56.6	5.4 to 6.9	9.4 to 24.7		271 to 446	5.9 to 8.4
Middle	C	60	−62.0 to −57.3	2.3 to 6.9	7.2 to 27.9		257 to 374	5.9 to 12.8
	W	65				−11.0 to −2.9	236 to 373	4.8 to 15.0
	S	7					245 to 314	34.4 to 39.3
	PC	45	−69.0 to −57.0		−30.0 to 26.7			
Late	W	67				−4.3 to −0.6	139 to 264	1.1 to 6.9

Note: $T_{m,CO2}$, final melting temperature of solid CO_2; $T_{m,cla}$, final melting temperature of the clathrate phase; $T_{h,CO2}$, temperature of CO_2 (L + V) to CO_2 (L); $T_{m,ice}$, final melting temperature of water ice; T_h, temperature of total homogenization of the inclusions; wt.% NaCl eqv., weight percentage of NaCl equivalent.

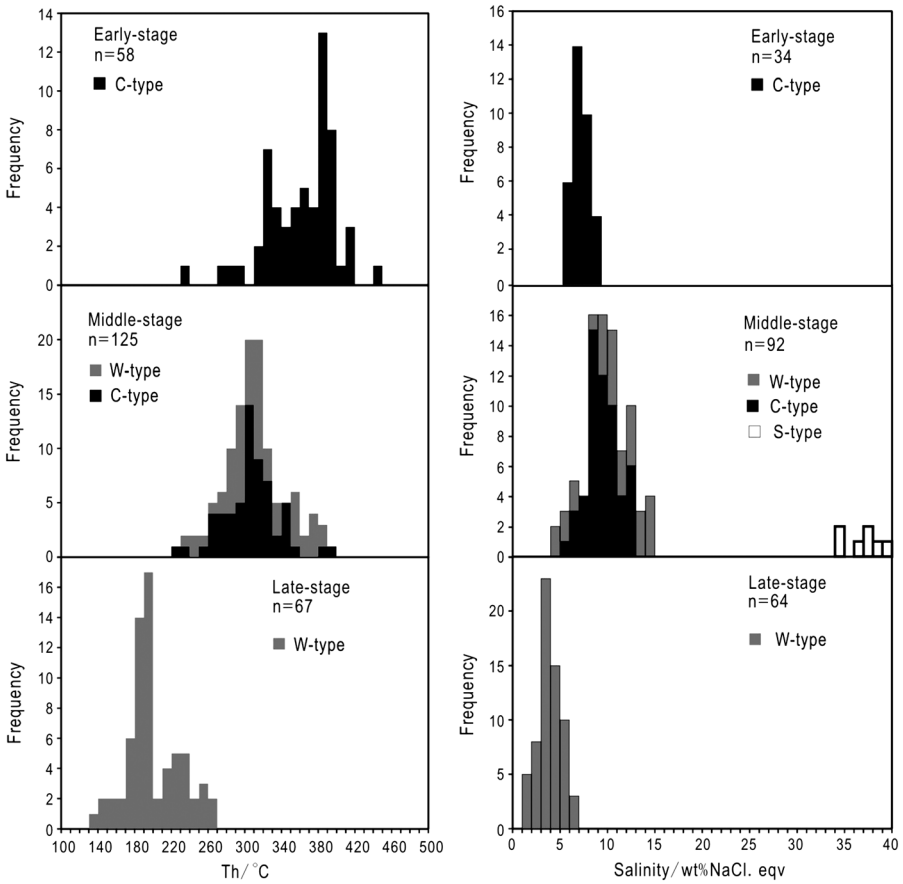

Figure 7. Total homogenization temperatures and salinities of fluid inclusions in different stages.

salinities from 34.4 to 39.3 wt.% NaCl eqv. PC-type inclusions yield melting temperatures for solid CO_2 from −69.0 to −57.0 °C. The homogenization temperatures of CO_2 to the liquid phase show a large variation from −30.0 to 26.7 °C, corresponding to densities from 0.68 to 0.98 g/cm^3.

In the late stage, only the W-type fluid inclusions can be observed in quartz veinlets. They contain less than 25% of vapour in volume at room temperature and are homogenized to liquid at temperatures from 139 to 264 °C. Their freezing points range from −4.3 to −0.6 °C, corresponding to salinities from 1.1 to 6.9 wt.% NaCl eqv., with densities varying from 0.86 to 0.92 g/m^3.

4.4. Laser Raman spectroscopy

Representative fluid inclusions were measured using laser Raman microspectroscopy to constrain their compositions. The analyses were performed in the Key Laboratory of

Mineralogy and Metallogeny, Chinese Academy of Sciences, Guangzhou. The wavelength of Ar^+ laser is 514.5 nm, and the measured spectrum time is 20 s. Counting rate is one time per centimetre. The spectrum diagram is taken from the wave band of 100–4000 cm^{-1}. The spectral resolution was ±2 cm^{-1} with a beam size of 1 μm. Instrumental settings were kept constant during all analyses.

The results show that most PC-type inclusions have obvious peaks of CO_2 (1282 and 1386 cm^{-1}), indicating that they contain pure CO_2. In some PC-type inclusions, the presence of CH_4 in the carbonic phase is evidenced by a sharp peak at 2913 cm^{-1} (Fig. 8A). The vapour and liquid phases of the W-type fluid inclusions are dominated by H_2O, but the vapour phase of some W-type inclusions contains a small amount of CO_2 or N_2 (Fig. 8B). The vapour phase of the C-type inclusions is dominated by CO_2, with minor CH_4 in some samples; and the liquid phases contain only H_2O (Fig. 8C).

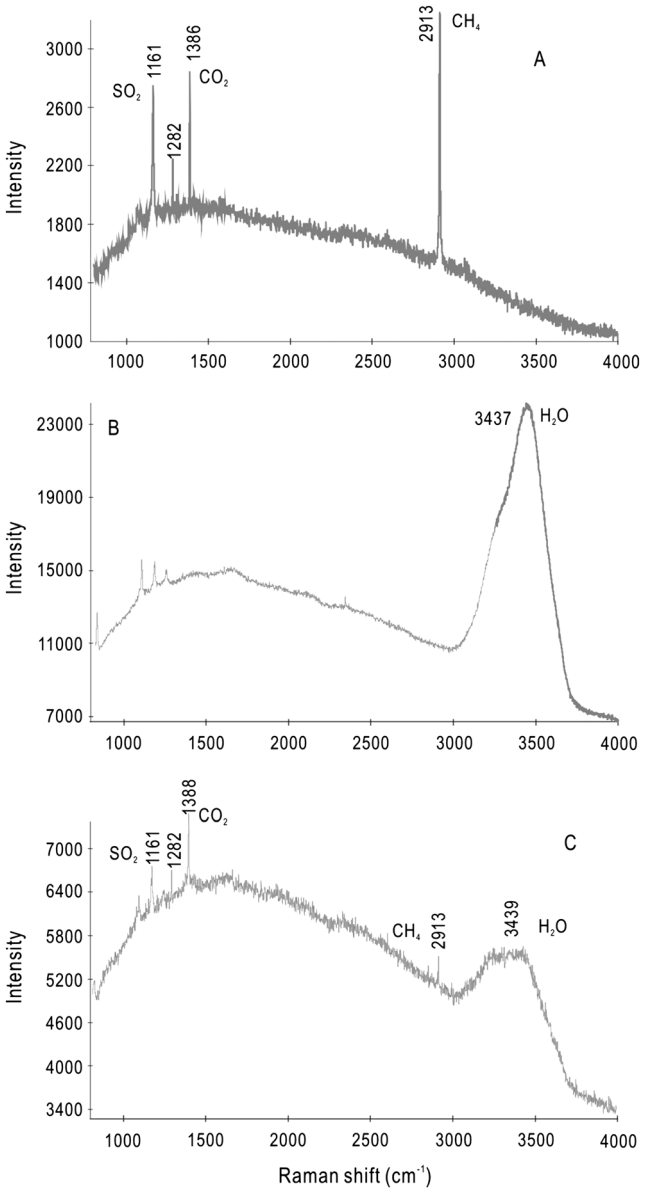

Figure 8. Laser Raman spectra of fluid inclusions: (**A**) CO_2 and CH_4 spectra of the PC-type fluid inclusion; (**B**) H_2O in liquid phase of W-type inclusion; (**C**) H_2O and CO_2 spectra of the vapour phase in C-type fluid inclusion.

5. Ar–Ar AGE

5.1. Sampling and analytical methods

One sample of mica for $^{40}Ar/^{39}Ar$ dating was collected from sulphide–quartz veinlets of the No. 1-1 orebody in the Sarekuobu deposit (Fig. 9). The sample was crushed to 20 mesh, from which the mica flakes were separated using conventional heavy liquid, magnetic techniques and ultrasonic cleaning. Finally, 0.2 g of mica of flakes was handpicked out under a binocular microscope to rule out the intergrowth.

Based on the chemical compositions analysed by EMPA, the calculated molecular formula of mica is $(K_{1.06}, Na_{0.02}, Ca_{0.01})_{1.09}(Fe_{1.4}, Mg_{1.19}, Al_{0.26}, Ti_{0.06})_{2.91}[(Si_{2.83}, Al_{1.17})_4O_{10}](OH_{1.99}, Cl_{0.01})_2$. Mg and Fe are the main cations, and $N(Mg) : N(Fe) < 2$, which can be identified as biotite.

Step-heating $^{40}Ar/^{39}Ar$ measurements were carried out using the MM-1200 and GV Instruments 5400 mass spectrometer at the Ar–Ar Laboratory of Guangzhou Institute of Geochemistry, Chinese Academy of Sciences. The detailed analytical techniques for MM-1200 and GV-5400 instruments have been described by Qiu and Wijbrans (2008). The $^{40}Ar/^{39}Ar$ results were calculated and plotted using the ArArCALC software (Koppers, 2002). The muscovite separates, together with the monitor standard DRA1 sanidine with an assumed age of 25.26 ± 0.07 Ma, wrapped in aluminium foil and shielded with cadmium foil, were irradiated with fast neutrons for 54 h at the Chinese Academy of Nuclear Energy Science, Beijing. Correction factors for interfering argon isotopes derived from Ca and K are $(^{39}Ar/^{37}Ar)_{Ca} = 8.984 \times 10^{-4}$, $(^{36}Ar/^{37}Ar)_{Ca} = 2.673 \times 10^{-4}$ and $(^{40}Ar/^{39}Ar)_K = 5.97 \times 10^{-3}$. The crusher consists of a 210 × 28 mm (in bore diameter) high-temperature resistant stainless steel tube (T_{max} is 1200 °C). The extraction and purification lines were baked out for about 10 h at 150 °C with a heating tape and the crusher at 250 °C with an external tube furnace. The blanks are ^{36}Ar (0.002–0.004) mV, ^{37}Ar (0.0002–0.0006) mV, ^{38}Ar (0.0004–0.0015) mV, ^{39}Ar (0.0025–0.0051) mV and ^{40}Ar (0.51–1.3) mV. The released gas was purified for 5–8 min by two Zr/Al getter pumps operating at room temperature and ~450 °C.

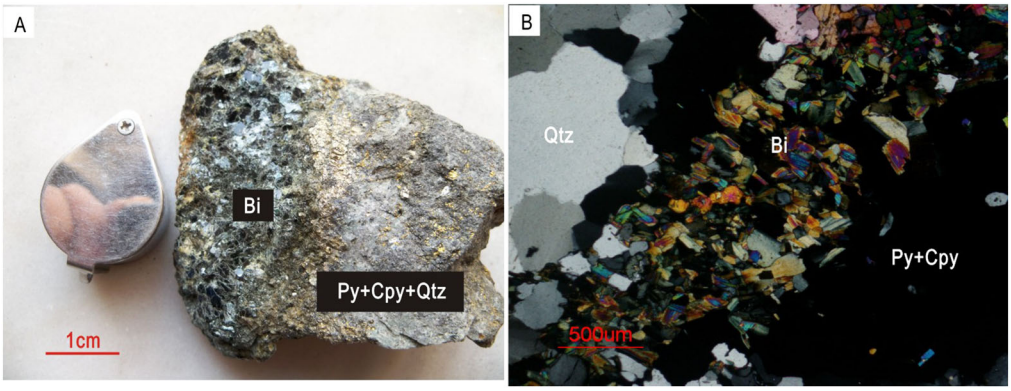

Figure 9. Photograph and microphotograph of micas at Sarekuobu: (**A**) biotite in the polymetallic–quartz vein; (**B**) biotite under crossed polarizers. Abbreviations: Qtz—quartz; Bi—biotite; Py—pyrite; Cpy—chalcopyrite. This figure is available in colour online at wileyonlinelibrary.com/journal/gj

5.2. *Results*

The $^{40}Ar/^{39}Ar$ analytical results are summarized in Table 2 and plotted in Figure 10. In this study, apparent ages obtained from $^{40}Ar/^{39}Ar$ analyses at low temperatures are not considered to have geological significance because of the low percentage of $^{39}Ar_k$ released, which was likely caused by the initial loss of small quantities of Ar from the edges of mineral grains. Plateau ages of this study were determined from six or more contiguous steps that comprise >80% of the total ^{39}Ar released. The uncertainties of the ages are reported at a 95% confidence level (2σ).

The sample yielded a plateau age of 213.5 ± 2.3 Ma (MSWD = 15.51) with 80% released gas of the ten steps. The inverse isochron yielded an age of 212.5 ± 2.2 Ma. The plateau age agrees with the isochron and inverse isochron ages, indicating that it is reliable with good quality. The initial $^{40}Ar/^{36}Ar$ ratio from the inverse isochron plot shows a value of 330.6 ± 16.4, slightly higher than, but almost consistent with the atmospheric value (295.5) within the analytical error. As a result, the 213.5 ± 2.3 Ma age for the sample is believed to be a reliable estimate of the crystallization age of biotite from the Sarekuobu ore, i.e. the mineralization occurred at about 213 Ma.

6. DISCUSSION

6.1. *Nature and evolution of fluids*

The four types of fluid inclusions at the Sarekuobu gold deposit suggest that the initial fluids were mesothermal (271–446 °C), low-salinity (5.9–8.4 wt.% NaCl eqv.) and CO_2-rich (CO_2–H_2O–NaCl ± N_2 ± CH_4) and evolved into a low-temperature (139–264 °C), low-salinity (1.1–6.9 wt.% NaCl eqv.) and CO_2-poor (H_2O–NaCl) system in the late

Table 2. $^{39}Ar/^{40}Ar$ stepwise laser ablation dating results of biotite

No.	$^{36}Ar(a)$	$^{37}Ar(Ca)$	$^{38}Ar(Cl)$	$^{39}Ar(K)$	$^{40}Ar(r)$	Age(Ma) ± 2σ		$^{40}Ar(\%)$	$^{39}Ar(\%)$
10G2166B	0.000409	0.000398	0.000007	0.002454	0.098901	225.30	±4.47	44.98	0.84
10G2166C	0.000549	0.000412	0.000014	0.007553	0.307660	227.60	±2.11	65.46	2.58
10G2166D	0.001402	0.001385	0.000029	0.014206	0.573150	225.56	±2.67	58.04	4.86
10G2166E	0.001606	0.000806	0.000026	0.012989	0.518720	223.41	±3.25	52.23	4.44
10G2166G	0.000541	0.000286	0.000031	0.016747	0.650083	217.52	±1.21	80.26	5.73
10G2166H	0.000333	0.000164	0.000039	0.022175	0.852478	215.54	±0.91	89.65	7.58
10G2166I	0.000370	0.000179	0.000064	0.038779	1.488829	215.27	±0.89	93.16	13.26
10G2166J	0.000144	0.000051	0.000047	0.029447	1.123857	214.06	±0.84	96.34	10.07
10G2166L	0.000039	0.000027	0.000028	0.018195	0.691707	213.28	±0.85	98.36	6.22
10G2166M	0.000061	0.000044	0.000060	0.036290	1.368414	211.64	±0.82	98.69	12.41
10G2166N	0.000048	0.000009	0.000040	0.025414	0.959063	211.80	±0.81	98.54	8.69
10G2166O	0.000030	0.000005	0.000020	0.013207	0.500510	212.65	±0.85	98.25	4.52
10G2166Q	0.000058	0.000030	0.000047	0.028357	1.083292	214.26	±0.83	98.43	9.69
10G2166R	0.000032	0.000061	0.000024	0.015428	0.582806	212.00	±0.85	98.42	5.27
10G2166S	0.000005	0.000000	0.000003	0.002011	0.074726	208.71	±1.22	97.90	0.69
10G2166T	0.000017	0.000007	0.000014	0.009119	0.357052	219.30	±0.88	98.63	3.12
10G2166U	0.000010	0.000014	0.000000	0.000137	0.007593	302.66	±9.55	72.90	0.05

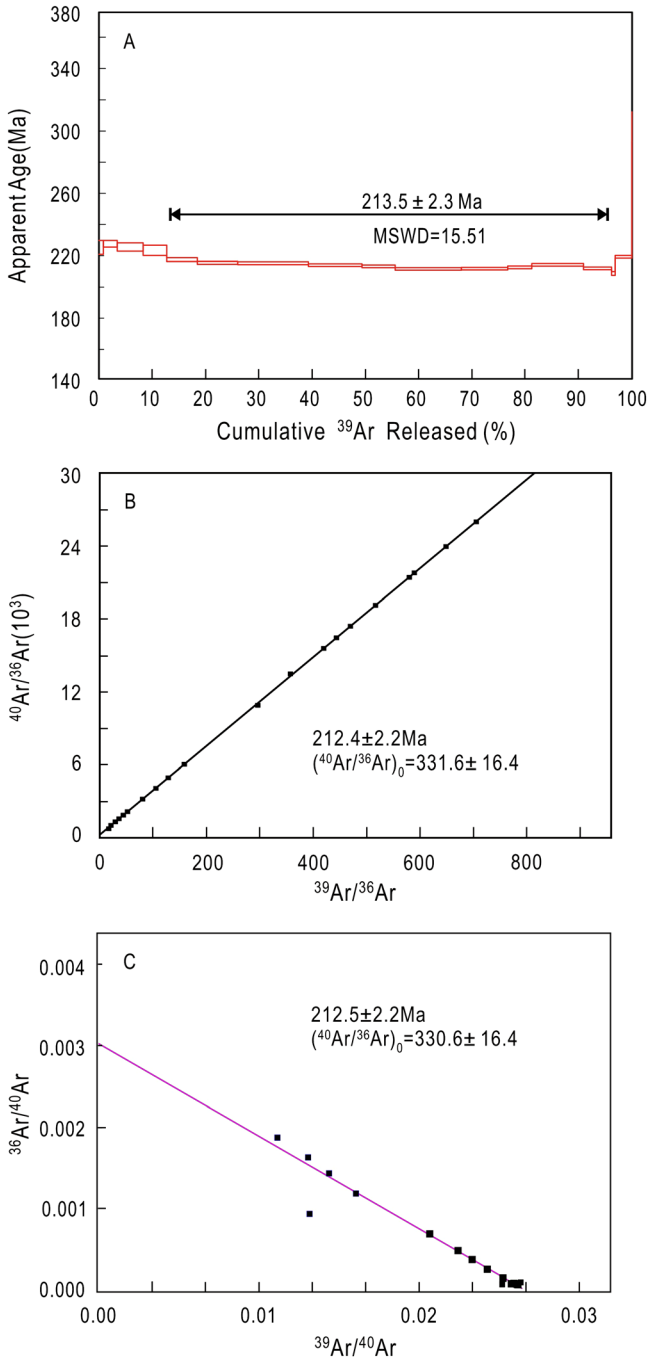

Figure 10. ^{40}Ar/^{39}Ar stepwise laser ablation data of biotite; (**A**) plateau age; (**B**) normal isochron; (**C**) inverse normal isochron. This figure is available in colour online at wileyonlinelibrary.com/journal/gj

stage. S-type fluid inclusions with high salinity appear to be co-genetic with W- and C-type inclusions with similar temperatures in the middle quartz–sulphide stage (Table 1). The W-type and C-type inclusions with different filling degrees appear to be coeval and show similar homogenization temperatures, even if they have different homogenization modes. These observations suggest that trapping of fluids was probably under boiling in the middle stage.

Due to the existence of boiling fluid inclusion assemblages, the pressure condition of fluid trapping during ore formation can be estimated. Trapping pressure of C-type inclusions of the middle stage was estimated at 90–250 MPa, based on homogenization temperatures and proportion of the CO_2 phase. The computation was done using the FLINCOR program (Brown, 1989) and equation of states for the H_2O–CO_2–NaCl system (Brown and Lamb, 1989). Given 1.0 g/cm^3 as a density of fluid and 2.7 g/cm^3 as an average density of rocks, this estimate suggests that the mineralization depth at Sarekuobu ranges up to 9 km in the middle stage, indicating that the mineralization was formed in a crustal uplift setting possibly caused by synorogenic crustal thickening.

Due to boiling, the salinities in the middle stage show a bimodal model characterized by two ranges of 34.4–39.3 and 4.8–15.0 wt.% NaCl eqv., respectively. Some W-type fluid inclusions with relatively low temperatures and salinities are present in the late quartz–calcite veinlets, which suggests that the addition of meteoric water to the hydrothermal system at Sarekuobu likely resulted in mixing and dilution of initial fluids, leading to a dominance of W-type fluid inclusions in the late stage of quartz vein formation (Kreuzer, 2005).

The boiling-resulted CO_2 escapes from the original homogeneous fluid phases in the middle stage, which led to the increase of pH values and the decrease of temperatures and then resulted in the precipitation of gold at Sarekuobu. This phenomenon of CO_2-loss and gold precipitation has been addressed in detail (Phillips and Evans, 2004; Y.J. Chen *et al.*, 2006) and observed at many orogenic-type gold deposits, e.g. the Wiluna Au–Sb deposit in Western Australia (Hagemann and Luders, 2003); the Sanshandao Au deposit in Jiaodong, China (Fan *et al.*, 2003); the Sawayaerdun Au–Sb deposit in Southwestern Chinese Tianshan (Chen *et al.*, 2012a, b); the Wangfeng Au deposit in Central Tianshan (Zhang *et al.*, 2012a); and the Yangshan (Li *et al.*, 2007), Huachanggou (Zhou *et al.*, 2014b), Wenyu (Zhou *et al.*, 2014a), Yindongpo (Zhang *et al.*, 2013) and Dahu (Ni *et al.*, 2014) gold deposits in the Qinling Orogen, China.

The ore-forming fluids at Sarekuobu are CO_2-rich with boiling feature, which are consistent with a metamorphic component (Chen *et al.*, 2007b; Pirajno, 2009). Fluids in the Sarekuobu gold deposit are generally similar to those of other mesothermal polymetallic deposits in the Abagong metallogenic belt, such as the Tiemurt Pb–Zn deposit and Wulasigou Cu deposit, in which their fluid sources have been also suggested to be metamorphic (Zheng *et al.*, 2012; Zhang *et al.*, 2012b; Zheng *et al.*, 2014).

6.2. *Timing of mineralization and tectonic application*

Field and petrographic relations indicate that biotite is closely related to gold mineralization, and thus, $^{40}Ar/^{39}Ar$ dating of biotite provides the constraints on the timing of hydrothermal alteration and gold deposition. Microthermometric measurements of primary fluid inclusions from auriferous quartz samples yielded final homogenization temperatures mostly between 260 and 320 °C, lower than the argon closure temperature for biotite at moderate cooling rates (350–400 °C; McDougall and Harrison, 1988). Consequently, the biotite $^{40}Ar/^{39}Ar$ age of 213.5 ± 2.3 Ma can be considered as the mineralization age for the Sarekuobu gold deposit.

The regional tectonic evolution of the Chinese Altay remains controversial (Xu *et al*., 2010). Felsic magmatism and large-scale shearing suggest that the collision of the Siberian Plate (Altay Terrane) and Kazakhstan Block (Junggar Terrane) occurred between the Early and Late Carboniferous (Li and Poliyangsiji, 2001; Li and Zhao, 2002; Yang *et al*., 2007). Palaeontological and palaeomagnetic studies argued for the Early Permian collision (Cocks and Torsvik, 2007). Xiao *et al*. (2008) proposed that formation of the complex orogenic collage between the Siberian Plate and Kazakhstan Block occurred between the Late Permian and Triassic, which is supported by our biotite Ar–Ar age and other evidence. Monazites from greenschist/amphibolite-grade meta-sediments in the Chinese Altay, dated by the chemical U–Th–Pb isochron method (CHIME), yield Permian metamorphic ages of 268–261 Ma that were interpreted by Zheng *et al*. (2007) as the time of metamorphism of subducted oceanic crust. They also believed that the metamorphism was related to the arc-continent collision. This is in good agreement with a group of SHRIMP U–Pb zircon ages and $^{40}Ar/^{39}Ar$ ages of 280–240 Ma of mafic granulites, granitic gneiss and mafic complex in the Chinese Altay (Li *et al*., 2004; Hu *et al*., 2006; H.L. Chen *et al*., 2006).

The facts addressed above indicate that a regional tectonothermal event in the Chinese Altay orogenic belt occurred from the Late Permian to the Triassic that may be related to the continental collision. The peak period of regional metamorphism associated with this collision was in the end of the Permian, which was usually followed by intensive hydrothermal activities and related mineralization documented in most orogenic-type deposits in the Qinling and Tianshan areas in China (Chen *et al*., 2004, 2012a, b, 2013; Zhang *et al*., 2012a, 2013; Yue *et al*., 2014; Zhou *et al*., 2014a, b).

6.3. *Ore genetic type of the Sarekuobu gold deposit*

Genetic models proposed for Sarekuobu include contrasting syngenetic and epigenetic interpretations. The previous syngenetic interpretation considered Sarekuobu as a volcanic-hosted massive sulphide (VHMS) deposit, based mainly on geological aspects such as the volcano-sedimentary host rocks of the deposit and stratabound character (Ding *et al*., 2001). However, the present data obtained in this study indicate that the Sarekuobu gold deposit is probably an epigenetic deposit belonging to an orogenic-type class (Groves *et al*., 1998; Goldfarb *et al*., 2001, 2005; Chen, 2006). The major lines of evidence leading to this conclusion include (1) Sarekuobu is a shear zone-hosted gold deposit with mineralization mainly occurring in quartz veins, quartz–fluorite veinlets and enclosing hydrothermal altered host rocks. (2) The abundant CO_2-rich fluid inclusions with low salinity commonly occurring in the quartz veins are characterized by metamorphic hydrothermal fluids, and in contrast to aqueous inclusions in VHMS-type deposits (Chen *et al*., 2007b). (3) The Ar–Ar plateau age (213.5 ± 2.3 Ma) of the mineralization at Sarekuobu obtained in this study remarkably postdates the zircon U–Pb ages of 421–396 Ma of the metamorphosed rhyolitic tuffs in the Kangbutiebao Formation (Chai *et al*., 2009; Shan *et al*., 2012; Zheng *et al*., 2013), which is considered as the host rocks of Sarekuobu. (4) The metallogenic events at Sarekuobu occurred in the Triassic (*ca.* 213 Ma), which is *ca.* 50 m.y. after the peak metamorphism of the host rocks. This fact is analogous to the typical orogenic-type deposits throughout the world (Chen *et al*., 2007b).

As a result, we can conclude that the Sarekuobu gold deposit was formed in a continental collisional setting that had occurred during the period from the Late Permian to the Triassic. Due to the collision, the strata were metamorphosed, devolatilized, thus triggered the formation of CO_2-rich ore-fluids in ore-forming systems of the Abagong ore belt including the Sarekuobu gold deposit. Similar characteristics on geology, geochemistry and geochronology were also recognized in the Tiemuert Pb–Zn deposit (Zhang *et al*., 2012b), the Wulasigou Cu deposit (Zhang *et al*., 2012b), the Keketale Pb–Zn–Cu deposit (Zheng *et al*., 2013) and the Qiaxia Cu–Fe deposit (Zheng *et al*., 2014), which indicate a coherent metamorphism-related metallogenic event occurred during the Late Permian to Triassic in the southern Chinese Altay.

7. CONCLUSIONS

Gold mineralization in the Sarekuobu gold deposit is hosted by Devonian volcanic-sedimentary rocks and is controlled by NW–SE trending shear zones. Ore-forming process includes the formation of early-stage quartz veins, middle-stage polymetallic sulphide–quartz veinlets and late-stage carbonate–quartz veinlets.

The aqueous, pure carbonic, carbonic-aqueous and solid-bearing fluid inclusions have been observed at the

Sarekuobu gold deposit, indicating that the deposit was formed by metamorphic fluids, instead of seafloor hydrothermal exhalation. The coexistence of carbonic, aqueous and solid-bearing fluid inclusions with similar homogenization temperatures in the middle-stage quartz shows that fluid boiling occurred and resulted in rapid precipitation of ore metals. The ore-forming fluid system evolved from CO_2-rich, metamorphic to late CO_2-poor, with significant input of meteoric fluids. The chemical composition, homogenization temperature, salinity and trapping pressure of fluid inclusions suggest a metamorphic source of the ore-forming fluids, rather than a seafloor hydrothermal exhalation system.

Biotite from the middle-stage polymetallic sulphide–quartz veinlet yields a $^{40}Ar/^{39}Ar$ plateau age of 213.5 ± 2.3 Ma, much later than that of the host rocks of the Kangbutiebao Formation. It is believed that the gold mineralization was related to the Permian–Triassic continental collision.

The geologic characteristics of the Sarekuobu gold deposit, fluid inclusions data and timing of the mineralization indicate that the Sarekuobu gold deposit belongs to the class of orogenic-type gold deposits, analogous to other deposits in the Abagong metallogenic belt.

ACKNOWLEDGEMENTS

The research was jointly supported by the National Basic Research Program of China (nos. 2014CB440802 and 2007CB411303) and the National Natural Science Foundation of China (nos. 41072062 and 41121002). We thank the Geological Team 706 of Xinjiang Bureau of Nonferrous Metals and Mr Chi Haogang for their help in field investigation. We also thank two anonymous reviewers for their useful comments and constructive reviews, which significantly improved the manuscript.

REFERENCES

Bodnar, R.J. 1993. Revised equation and table for determining the freezing point depression of H_2O–NaCl solutions. *Geochimica et Cosmochimica Acta* **57**, 683–684.

Brown, P.E. 1989. Flincor: a microcomputer program for the reduction and investigation of fluid-inclusion data. *American Mineralogist* **74**, 1390–1393.

Brown, P.E. Lamb, W.M. 1989. P-V-T properties of fluids in the system $H_2O \pm CO_2 \pm$ NaCl: new graphic presentations and implications for fluid inclusion studies. *Geochimica et Cosmochimica Acta* **53**, 1209–1221.

Chai, F.M., Mao, J.W., Dong, L.H., Yang, F.Q., Liu, F., Geng, X.X., Zhang, Z.X. 2009. Geochronology of metarhyolites from the Kangbutiebao Formation in the Kelang basin, Altay Mountains, Xinjiang: implications for the tectonic evolution and metallogeny. *Gondwana Research* **16**, 189–200.

Chen, H.L., Yang, S.F., Yuan, C., Xiao, W.J., Li, J.L., Yu, X., Lin, X.B. 2006. Tectonic setting of mafic rocks in southern Altay orogenic belt and its geodynamic implication. *Acta Petrologica Sinica* **22**, 127–134.

Chen, H.Y., Chen, Y.J., Liu, Y.L. 2001. Metallogenesis of the Ertix gold belt, Xinjiang and its relationship to Central Asia-type orogenesis. *Science in China Series D* **44**, 245–255.

Chen, H.Y., Chen, Y.J., Baker, M.J. 2012a. Evolution of ore-forming fluids in the Sawayaerdun gold deposit in the Southwestern Chinese Tianshan metallogenic belt, Northwest China. *Journal of Asian Earth Sciences* **49**, 131–144.

Chen, H.Y., Chen, Y.J., Baker, M.J. 2012b. Isotopic geochemistry of the Sawayaerdun orogenic-type gold deposit, Tianshan, northwest China: implications for ore genesis and mineral exploration. *Chemical Geology* **310-311**, 1–11.

Chen, H.Y., Zhang, L., Li, D.F., Zhang, Z.J. 2013. Characteristics of rare earth and trace elements of the Sawayaerdun gold deposit, Southwest Tianshan: implications for ore genesis. *Acta Petrologica Sinica* **29**, 159–166 (in Chinese with English abstract).

Chen, Y.J. 2000. Progress in the study of Central Asia-type orogenesis–metallogenesis in Northwest China. *Geological Journal of China Universities* **6**, 17–22 (in Chinese).

Chen, Y.J. 2006. Orogenic-type deposits and their metallogenic model and exploration potential. *Geology China* **33**, 1181–1196 (in Chinese with English abstract).

Chen, Y.J., Pirajno, F., Sui, Y.H. 2004. Isotope geochemistry of the Tieluping silver deposit, Henan, China: a case study of orogenic silver deposit and related tectonic setting. *Mineralium Deposita* **39**, 560–575.

Chen, Y.J., Pirajno, F., Qi, J.P., Li, J., Wang, H.H. 2006. Ore geology, fluid geochemistry and genesis of the Shanggong gold deposit, eastern Qinling Orogen, China. *Resource Geology* **56**, 99–116.

Chen, Y.J., Chen, H.Y., Zaw, K., Pirajno, F., Zhang, Z.J. 2007a. Geodynamic settings and tectonic model of skarn gold deposits in China: an overview. *Ore Geology Reviews* **31**, 139–169.

Chen, Y.J., Ni, P., Fan, H.R., Pirajno, F., Lai, Y., Su, W.C., Zhang, H. 2007b. Diagnostic fluid inclusions of different types hydrothermal gold deposits. *Acta Petrologica Sinica* **23**, 2085–2108 (in Chinese with English abstract).

Chen, Y.J., Zhai, M.G., Jiang, S.Y. 2009. Significant achievements and open issues in study of orogenesis and metallogenesis surrounding the North China continent. *Acta Petrologica Sinica* **25**, 2695–2726 (in Chinese with English abstract).

Chen, Y.J., Pirajno, F., Wu, G., Qi, J.P., Xiong, X.L. 2012. Epithermal deposits in North Xinjiang, NW China. *International Journal of Earth Sciences* **101**, 889–917.

Cocks, L.R.M., Torsvik, T.H. 2007. Siberia, the wandering northern terrane, and its changing geography through the Palaeozoic. *Earth-Science Reviews* **82**, 29–74.

Collins, P.L.F. 1979. Gas hydrates in CO_2-bearing fluid inclusions and use freezing data for estimation of salinity. *Economic Geology* **74**, 1435–1444.

Ding, R.F., Wang, J.B., Ma, Z.M., Zhang, J.H., Fang, T.H. 2001. Geochemical character of the Sarekoubu volcanic exhalation–sedimentary–superimposition gold deposit in Xinjiang. *Geology and Prospecting* **37**, 11–15 (in Chinese with English abstract).

Fan, H.R., Zhai, M.G., Xie, Y.H., Yang, J.H. 2003. Ore-forming fluids associated with granite-hosted gold mineralization at the Sanshandao deposit, Jiaodong gold province, China. *Mineralium Deposita* **38**, 739–750.

Geological Team 706 of the Xinjiang Bureau of Nonferrous Metals, 2000. *Prospecting report of the Tiemurt Ore Belt, Altay, Xinjiang Uygur Autonomous Region*. Geological Team 706 of the Xinjiang Bureau of Nonferrous Metals; Altay (Unpublished Document, in Chinese).

Goldfarb, R.J., Groves, D.I., Cardoll, S. 2001. Orogenic Au and geologic time: a global synthesis. *Ore Geology Reviews* **18**, 1–75.

Goldfarb, R.J., Mao, J.W., Hart, C., Wang, D., Anderson, E., Wang, Z. 2003. Tectonic and metallogenic evolution of the Altay Shan, Northern Xinjiang Uygur Autonomous Region, northwestern China. In: *Tectonic Evolution and Metallogeny of the Chinese Altay and Tianshan*, Mao, J.W., Goldfarb, R.J., Seltmann, R., Wang, D.H., Xiao, W.J., Hart, C. (eds). International Association on the Genesis of Ore Deposits, Centre for Russian and Central Asian Mineral Studies. Natural History Museum: London; 17–30.

Goldfarb, R.J., Baker, T., Dube, B., Groves, D.I., Hart, C.J.R., Gosselin, P. 2005. Distribution, character, and genesis of gold deposits in metamorphic terranes. *Economic Geology* 100th Anniversary Volume, 407–450.

Groves, D.I., **Goldfarb, R.J.**, **Gebre-Mariam, M.**, **Hagemann, S.G.**, **Robert, F. 1998**. Orogenic gold deposits: a proposed classification in the context of their crustal distribution and relationship to other gold deposit types. *Ore Geology Reviews* **13**, 7–27.

Hagemann, S.G., **Luders, V. 2003**. *P-T-X* conditions of hydrothermal fluids and precipitation mechanism of stibnite–gold mineralization at the Wiluna lode-gold deposits, Western Australia: conventional and infrared microthermometric constraints. *Mineralium Deposita* **38**, 936–952.

Hall, D.L., **Sterner, S.M.**, **Bodnar, R.J. 1988**. Freezing-point depression of NaCl–KCl–H_2O solutions. *Economic Geology* **83**, 197–202.

Hu, A.Q., **Wei, G.J.**, **Deng, W.F.**, **Chen, L.L. 2006**. SHRIMP zircon U–Pb dating and its significance for gneisses from the southwest area to Qinghe County in the Altai, China. *Acta Petrologica Sinica* **22**, 1–10 (in Chinese with English abstract).

Koppers, A.A.P. 2002. ArArCALC-software for $^{40}Ar/^{39}Ar$ age calculations. *Computers and Geosciences* **28**, 605–619.

Kreuzer, O. 2005. Intrusion-hosted mineralization in the Charters Towers Goldfield, North Queensland: new isotopic and fluid inclusion constraints on the timing and origin of the auriferous veins. *Economic Geology* **100**, 1583–1603.

Li, J., **Chen, Y.J.**, **Li, Q.Z.**, **Lai, Y.**, **Yang, R.S.**, **Mao, S.D. 2007**. Fluid inclusion geochemistry and genetic type of the Yangshan gold deposit, Gansu, China. *Acta Petrologica Sinica* **23**, 2144–2154 (in Chinese with English abstract).

Li, T.D., **Poliyangsiji, B.H. 2001**. Tectonics and crustal evolution of Altai in China and Kazakhstan. *Xinijang Geology* **19**, 27–32 (in Chinese with English abstract).

Li, Z.L., **Chen, H.L.**, **Yang, S.F.**, **Dong, C.W.**, **Xiao, W.J.**, **Li, J.L.**, **Ye, Y.**, **Wang, J. 2004**. Discovery and genetic mechanism of basic granulite in the Altay orogenic belt, Xinjiang, NW China. *Acta Petrologica Sinica* **78**, 177–185 (in Chinese with English abstract).

Li, Z.W., **Zhao, Z.Z. 2002**. Creation of the Altai orogenic belt and the Altai metals tectono-metallogenic province. *Chinese Journal of Geology* **37**, 101–108 (in Chinese with English abstract).

McDougall, I., **Harrison, T. 1988**. *Geochronology and Thermochronology by ^{40}Ar–^{39}Ar Method*. Oxford University Press: London; 1–212.

Ni, Z.Y., **Li, N.**, **Zhang, H. 2014**. Hydrothermal mineralization at the Dahu Au-Mo deposit in the Xiaoqinling gold field, Qinling Orogen, central China. *Geological Journal* **49**(4–5), 501–514. DOI: 10.1002/gj.2564

Phillips, G.N., **Evans, K.A. 2004**. The role of CO_2 in the formation of gold deposits. *Nature* **429**, 860–863.

Pirajno, F. 2009. *Hydrothermal Processes and Mineral System*. Springer: Berlin; 1–1250.

Qin, Y.J., **Zhang, L.**, **Zheng, Y.**, **Liu, C.F.**, **Chi, H.G. 2012**. Fluid inclusion studies and the genesis of the Sarekuobu gold deposit, Xinjiang. *Geotectonica et Metallogenia* **36**, 227–239 (in Chinese with English abstract).

Qiu, H.N., **Wijbrans, J.R. 2008**. The Paleozoic metamorphic history of the Central Orogenic Belt of China from $^{40}Ar/^{39}Ar$ geochronology of eclogite garnet fluid inclusions. *Earth and Planetary Science Letters* **268**, 501–514.

Sengor, A.M.C., **Natal'in, B.A. 1996**. Paleotectonics of Asia: fragments of synthesis. In: *The Tectonic Evolution of Asia,* Yin, A., Harrison, T.M. (eds). Cambridge University Press: Cambridge; 480–640.

Shan, Q., **Zeng, Q.S.**, **Li, N.B.**, **Yang, W.B.**, **Luo, Y.**, **Jiang, Y.H.**, **Yu, X. Y. 2012**. Zircon U–Pb ages and geochemistry of the potassic and sodic rhyolites of the Kangbutiebao Formation in the southern margin of Altay, Xinjiang. *Acta Petrologica Sinica* **28**, 2132–2144 (in Chinese with English abstract).

Tong, M.Y. 2007. Geological characteristics and Genesis of Tiemierte Pb–Zn deposit. *Xinjiang Nonferrous Metal* Supplementary Issue, 42–44 (in Chinese).

Wang, J.B., **Qin, K.Z.**, **Wu, Z.L.**, **Hu, J.H.**, **Deng, J.N. 1998**. *Volcanic–Exhalative–Sedimentary Lead Zinc Deposit in the Southern Margin of the Altai, Xinjiang*. Geology Publishing House: Beijing; 1–210 (in Chinese).

Wang, L.L., **Xu, J.H.**, **Sun, F.Y.**, **Lin, L.H.**, **Chu, H.X. 2012**. Two types of mineralization and genesis in Sarekoubu–Tiemurte area of Altay Xinjiang. *Global Geology* **31**, 100–112 (in Chinese with English abstract).

Wang, S.L., **Chen, K.Q.**, **Kang, J.C.**, **Guo, Q. 2007**. Stable isotope of Pb–Zn deposits occurred in the Maizi Devonian volcanic-sedimentary basin in the south margin of Altay mountain, Xinjiang. *Geology and Prospecting* **43**, 25–31 (in Chinese with English abstract).

Xiao, W.J., **Han, C.M.**, **Yuan, C.**, **Sun, M.**, **Lin, S.F.**, **Chen, H.L.**, **Li, Z. L.**, **Sun, S. 2008**. Middle Cambrian to Permian subduction-related accretionary orogenesis of Northern Xinjiang, NW China: implications for the tectonic evolution of central Asia. *Journal of Asian Earth Sciences* **32**, 102–117.

Xiao, W.J., **Windley, B.F.**, **Huang, B.C.**, **Han, C.M.**, **Yuan, C.**, **Chen, H. L.**, **Sun, M.**, **Sun, S.**, **Li, J.L. 2009**. End-Permian to mid-Triassic termination of the southern Altaids: implications for the geodynamic evolution, Phanerozoic continental growth, and metallogeny of Altay Asia. *International Journal of Earth Sciences* **98**, 1189–1217.

Xu, J.H., **Ding, R.F.**, **Wei, X.F.**, **Zhong, C.H.**, **Shan, L.H. 2008**. The source of hydrothermal fluids for Sarekoubu gold deposit in the southern Altai Mountains in Xinjiang, China: evidence from fluid inclusions and geochemistry. *Journal of Asian Earth Sciences* **32**, 247–258.

Xu, J.H., **Graig, H.**, **Wang, L.L.**, **Chu, H.X.**, **Ding, R.F.**, **Lin, L.H.**, **Wei, X.F. 2011**. Carbonic fluid overprints in volcanogenic massive sulfide deposits: examples from the Kelan volcanosedimentary basin, Altaids, China. *Economic Geology* **106**, 145–158.

Xu, L.G., **Mao, J.W.**, **Yang, F.Q.**, **Daniel, H.**, **Zheng, J.M. 2010**. Geology, geochemistry and age constraints on the Mengku skarn iron deposit in Xinjiang Altay, NW China. *Journal of Asian Earth Sciences* **39**, 423–440.

Yang, F.Q., **Mao, J.W.**, **Xu, L.G.**, **Zhang, Y.**, **Liu, F.**, **Huang, C.L.**, **Liu, G.R.**, **Dai, J.Z. 2007**. REE geochemistry and the indication for iron mineralization of Mengku iron deposit in Xinjiang. *Acta Petrologica Sinica* **23**, 2443–2456 (in Chinese with English abstract).

Yue, S.W., **Deng, X.H.**, **Bagas, L. 2014**. Geology, isotope geochemistry and ore genesis of the Yindonggou Ag–Au(–Pb–Zn) deposit, Hubei Province, China. *Geological Journal* **49**(4–5), 442–462. DOI: 10.1002/gj.2561

Zhang, J., **Chen, Y.J.**, **Pirajno, F.**, **Deng, J.**, **Chen, H.Y. 2013**. Geology, isotope systematics and ore genesis of the Yindongpo gold deposit, Tongbai Mountains, central China. *Ore Geology Reviews* **53**, 343–356.

Zhang, L., **Chen, H.Y.**, **Chen, Y.J.**, **Qin, Y.J.**, **Liu, C.F.**, **Zheng, Y.**, **Nicholas H.J. 2012a**. Geology and fluid evolution of the Wangfeng orogenic-type gold deposit, Western Tian Shan, China. *Ore Geology Reviews* **49**, 85–95.

Zhang, L., **Zheng, Y.**, **Chen, Y.J. 2012b**. Ore geology and fluid inclusion geochemistry of the Tiemurt Pb–Zn–Cu deposit, Altay, Xinjiang, China: a case study of orogenic-type Pb–Zn systems. *Journal of Asian Earth Sciences* **49**, 69–79.

Zheng, C.Q., **Kato, T.**, **Enami, M.**, **Xu, X.C. 2007**. CHIME monazite ages of metasediments from Altai orogen in northwestern China: Devonian and Permian ages of metamorphism and their significance. *Island Arc* **16**, 598–604.

Zheng, Y., **Zhang, L.**, **Chen, Y.J.**, **Qin, Y.J.**, **Liu, C.F. 2012**. Geology, fluid inclusion geochemistry, and $^{40}Ar/^{39}Ar$ geochronology of the Wulasigou Cu deposit, and their implications for ore genesis, Altay, Xinjiang, China. *Ore Geology Reviews* **49**, 128–140.

Zheng, Y., **Zhang, L.**, **Guo, Z.L. 2013**. Zircon LA-ICP-MS U–Pb and biotite $^{40}Ar/^{39}Ar$ geochronology of the Tiemurt Pb–Zn–Cu deposit, Xinjiang: implications for the ore genesis. *Acta Petrologica Sinica* **29**, 191–204.

Zheng, Y., **Zhang, L.**, **Chen, H.Y.**, **Li, D.F.**, **Wang, C.M.**, **Fang, J. 2014**. CO_2-rich fluids from metamorphic devolatilization of the Triassic Orogeny: an example from the Qiaxia Copper deposit in Altay, NW China. *Geological Journal* **49**(6), 617–634. DOI: 10.1002/gj.2536

Zhou, Z.J., **Chen, Y.J.**, **Jiang, S.Y.**, **Zhao, H.X.**, **Qin, Y.**, **Hu, C.J. 2014a**. Geology, geochemistry and ore genesis of the Wenyu gold deposit, Xiaoqinling gold field, southern margin of North China Craton. *Ore Geology Reviews* **59**, 1–20.

Zhou, Z.J., **Lin, Z.W.**, **Qin, Y. 2014b**. Geology, geochemistry and genesis of the Huachanggou gold deposit, western Qinling Orogen, central China. *Geological Journal* **49**(6), 424–441. DOI: 10.1002/gj.2557

